Materials Chemistry and Physics 259 (2021) 124011

Contents lists available at ScienceDirect

Materials Chemistry and Physics

journal homepage: www.elsevier.com/locate/matchemphys

Petroleum waste hydrocarbon resin as a carbon source modified on a Si composite as a superior anode material in lithium ion batteries

Wen-Ya Chung [a,1], Sanjaya Brahma [a,e,1], Shang-Chieh Hou [b,e,f], Chia-Chin Chang [b,c,e,**], Jow-Lay Huang [a,d,e,*]

[a] Department of Materials Science and Engineering, National Cheng Kung University, Tainan, 701, Taiwan
[b] R & D Center for Li-ion Battery, National University of Tainan, Tainan, 70005, Taiwan
[c] Department of Greenergy, National University of Tainan, Tainan, 70005, Taiwan
[d] Center for Micro/Nano Science and Technology, National Cheng Kung University, Tainan, 701, Taiwan
[e] Hierarchical Green-Energy Materials (Hi-GEM) Research Center, National Cheng Kung University, Tainan, 701, Taiwan
[f] Electric Motor Technology Research Center, National Cheng Kung University, Tainan, Taiwan

HIGHLIGHTS

- Investigation of Si/C composite as anode in lithium ion battery.
- The composite is synthesized by using petroleum waste hydrocarbon resin as carbon source.
- Significant discharge capacity (1402 $mAhg^{-1}$) is achieved after 100 charge/discharge cycles.
- Excellent electrochemical performance due to the formation of C, SiOC/SiOx layer over the Si.
- Si/C composite could be suitable to replace conventional graphite anode.

GRAPHICAL ABSTRACT

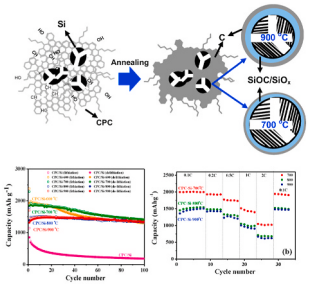

ARTICLE INFO

Keywords:
Si/C composite
Anode material
Lithium ion battery
Planetary ball-milling/heat treatment

ABSTRACT

We demonstrate impressive electrochemical performance of a silicon(Si)/carbon(C) composite prepared by mixing an appropriate concentration of hydrocarbon resin, Si powder, and polyacrylic acid followed by a simple ball milling process and heat treatment at temperatures ranging from 600°C to 900 °C. The Si/C composite annealed at 700 °C achieved a significantly high discharge capacity (2291 mAh g^{-1}) in the first cycle, very good cyclic stability (1402 mAh g^{-1} after 100 cycles), and excellent rate capability (1020 mAh g^{-1} at 2C with a retention of 95.5%). The composites annealed at high temperatures (800 °C and 900 °C) also displayed good capacity (1330 mAh g^{-1}, 1340 mAh g^{-1}) after 100 cycles and high rate capability (676 mAh g^{-1}, 619 mAh g^{-1} @2C). indicating outstanding physical/chemical/structural stability of the composite that makes it a very suitable anode material in lithium ion batteries. The annealing temperature led to the formation of a C, SiOC/SiOx layer over the Si, as observed through a microstructure analysis, and different degrees of oxidation of the Si were observed using X-ray photoelectron spectroscopy. A detailed, comprehensive analysis of the structure/microstructure, bond vibrations, oxidation states of Si, and electrochemical performance is carried out.

* Corresponding author. Department of Materials Science and Engineering, National Cheng Kung University, Tainan, 701, Taiwan.
** Corresponding author. R & D Center for Li-ion Battery, National University of Tainan, Tainan, 70005, Taiwan.
E-mail addresses: ccchang@mail.nutn.edu.tw (C.-C. Chang), jlh888@mail.ncku.edu.tw (J.-L. Huang).
[1] The authors (Wen-Ya Chung, Sanjaya Brahma) have contributed equally.

https://doi.org/10.1016/j.matchemphys.2020.124011
Received 31 July 2020; Received in revised form 28 October 2020; Accepted 3 November 2020
Available online 12 November 2020
0254-0584/

1. Introduction

Research to develop negative (anode) electrode materials in lithium ion batteries (LIBs) is an emerging topic due to the large-scale production/usage of consumer electronic devices, electronic appliances, and medical devices (e.g. thermometer) and to meet the huge demand for electric hybrid vehicles. The currently produced LIBs typically use graphite (specific capacity = 372 mAh g^{-1}) as the anode to run portable electronic devices; however, for higher-end applications, it is essential to develop anode materials with significantly higher capacity, excellent cyclic stability, high energy density, and much better rate capabilities. Recently, silicon (Si) has been at the forefront of the research [1–5] for its possible application as an anode material in LIBs due to its distinct theoretical capacity (4200 mAh g^{-1}), which may be a suitable alternative for graphite (~372 mAh g^{-1}) or metal oxide (~1000 mAh g^{-1}) [6–11] due to the added advantages of a low discharge voltage (~0.4 V versus Li^{+}/Li) and availability. However, excessive volume expansion (~400%) is a major concern that leads to cracking and deterioration of the electrode due to the significant growth of the solid electrolyte interface (SEI) layer, as well as electrolyte decomposition that eventually affects the columbic efficiency, reduce electronic conductivity for the ion transport, and causes capacity fading and cyclic stability. Efforts have been undertaken to prepare Si nanoparticles [12], nanowires [13], nanotubes [14], hollow nanospheres [15], and porous Si nanowires [16], for which the electrochemical performance has been impressive (3500 mAh g^{-1} after 20 cycles, ~3000 mAh g^{-1} after 200 cycles). Composites of Si with metal oxides [17], carbon [12,18–26], graphene [27,28] and metal alloys [29–34] with Si have also been synthesized, and the anode performance of the composite has been tested.

Si–C nanocomposites are of considerable interest since carbon is a unique material with excellent electrical and mechanical properties that enhances the electrical conductivity and the structural integrity of the silicon anodes and thereby establishes effective electrical contact and prevents SEI formation. In addition, carbonaceous materials may generate additional lithium storage sites and can act as a buffer to accommodate the volume expansion of Si without damaging the carbon layer [12,18,23,35]. Pan et al. [23] synthesized a Si–C core shell structure using an easy, scalable method, and the composite achieved good capacity (804 mAh g^{-1}) at a high rate (1 Ag^{-1}) after 50 cycles. Similar core-shell structures have also been synthesized by Li et al. [35] and Liu et al. [21], where the Si–C nanocomposites with void spaces up to tens of nanometers intended to accommodate the volume expansion during lithiation led to good capacity retention (760 mA h g^{-1} @ 1 A g^{-1} after 100 cycles, 1500 mAh g^{-1} @ 1C after 1000 cycles). Magasinski et al. [20] used chemical vapor deposition (CVD) to prepare Si nanoparticles on the surface of carbon black nanoparticles, which were found to have good capacity (~1600 mAh g^{-1}) after 100 cycles. Shao et al. [22] prepared a nanostructured silicon/porous carbon spherical composite using a simple hydrothermal method, where silicon nanoparticles were coated with a porous carbon shell. The composite delivered satisfactory capacity (1050 mA h g^{-1}) at a very high current density (10 A g^{-1}). Synthesis of Si–C composites includes mixing of poly(styrene) (PS) resin with Si using high energy ball milling [18], growth of carbon nanotubes on Ni–P/Si particles by high temperature decomposition of acetylene [19], and growth of Si nanoparticles on carbon black particles using CVD [20]. Si–C core shell structures [21] are synthesized using a room temperature solution method, where Si nanoparticles are first coated with a SiO_2 sacrificial layer and subsequently with a polydopamine layer, the carbonization of which produces an N-doped C coating. Subsequent removal of the SiO_2 layer with hydrofluoric acid (HF) leads to the production of a yolk-shell Si@void@C structure. All these very impressive results have inspired revisiting and carrying out further experiments on Si/C composites.

Here, we demonstrate the use of hydrocarbon resin for the synthesis of an Si-carbon composite prepared using planetary ball milling followed by annealing at different temperatures (600°C–900 °C). The Si/C composite annealed at 700 °C exhibited impressive discharge capacity (1402 mAh g^{-1}) after 100 charge/discharge cycles as well as high rate capability (~1400 mAh g^{-1} @1C). Additionally, hydrocarbon resin reacts with highly reactive surface Si dangling bonds resulting from high-energy mechanical milling [36,37], inducing the SiOx/SiOC formation, in particular, at high annealing temperatures (>800 °C). An SiOx/SiOC layer coated on Si further enhances the integrity of the Si/C composite during charge/discharge cycles, resulting in excellent capacity retention after 100 cycles.

2. Experimental procedure

The chemicals used for the synthesis of the CPC/Si composite included hydrocarbon resin from petroleum waste (CPC Co) and high energy mechanically-milled and wet-milled silicon powder (Si $_{H+W}$) [38], polyacrylic acid (PAA, Sigma-Aldrich Co), and ethanol

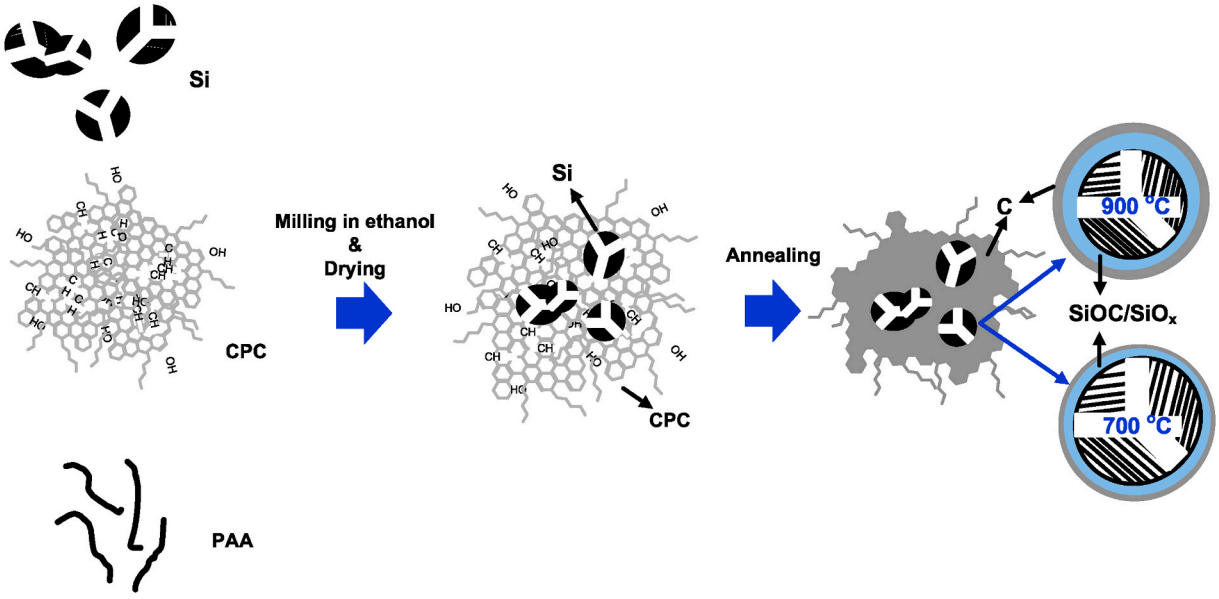

Scheme 1. Procedure for preparing CPC-Si composite.

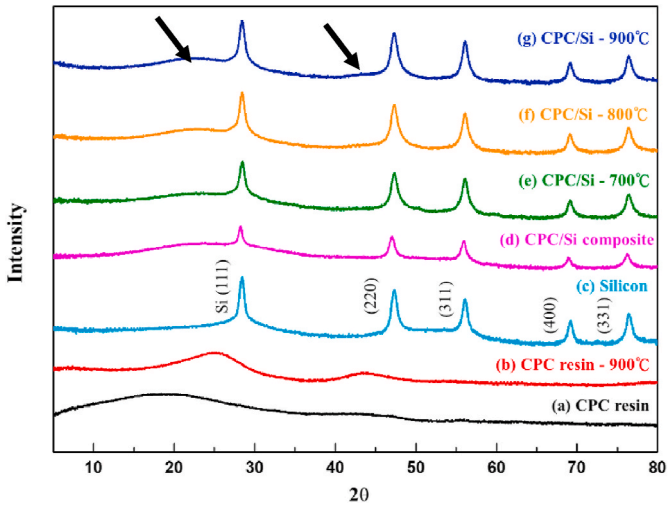

Fig. 1. XRD spectra of (a) CPC resin, (b) CPC resin-900 °C, (c) silicon (Si), (d) CPC/Si composite, (e) CPC/Si-700 °C, (f) CPC/Si-800 °C, and (g) CPC/Si-900 °C. (For interpretation of the references to color in this figure legend, the reader is referred to the Web version of this article.)

(Sigma-Aldrich Co). The chemical formula of the petroleum waste hydrocarbon resin and the composition derived from the crude oil as declared by the vendor is $C_{176}H_{148}O$, composed of C (92.5 wt%), H (6.0 wt%), O (0.6 wt%), N (0.05 wt%) and S (0.3 wt%). In a typical procedure, the powders were prepared by mixing 45 wt% CPC resin, 45 wt % silicon powders, and 10 wt% poly acrylic acid. The powder mixture was then subjected to solid-state ball milling in a planetary mixer (power Mixer-S, Chia Mey Machinery Co.) at 800 rpm for 60 min followed by the addition of 95 wt% ethanol for wet milling at 800 rpm for 60 min. The composite was dried in an oven at 90 °C for 6 h and annealed at different temperatures (600°C–900 °C) for 2 h in an argon atmosphere. The synthesis procedure is described by a schematic diagram (Scheme 1).

2.1. Characterization of the CPC/Si composite

X-ray diffraction (Bruker AXS Gmbh, Karlsruhe, Germany) was used to determine the crystallinity and crystallographic structure of the CPC resin and CPC/Si composite using Cu Kα radiation at an angular speed of 3° (2θ)/min with 2θ from 5° to 80°. The microstructure was observed using high-resolution field emission scanning electron microscopy (HR-FESEM) and ultrahigh resolution analytical electron spectroscopy (HR-AEM). Variations in the oxygen-containing CPC/Si composite functional group were confirmed using Raman and FTIR spectrometry. The energy levels of the carbon and silicon in the CPC/Si composite were confirmed with an electron spectroscopy chemical analysis (ESCA).

2.2. Electrochemical analysis

The slurry was prepared by combining the solid components as 65 wt % active materials, 20 wt% Super P (MMM Carbon, Belgium), 9 wt% poly (acrylic acid) (PAA, Sigma-Aldrich Co.), 3.5 wt% styrene butadiene rubber (SBR, Zeon Co.), and 2.5 wt% carboxymethyl cellulose (CMC, Sigma-Aldrich Co.). Mixing was performed in a planetary mixer (G-Mixer 400S, Gold Max Applied Materials Co.). The electrodes were prepared by casting the slurry onto a sheet of copper foil (Nippon Foil Co.) following by drying in an oven at 90 °C for 1 h. The composite anode was stored in a glove box (with oxygen and humidity maintained below 10 ppm) for more than 24 h before electrochemical testing. For the cycle test, the cells underwent galvanostatic charge/discharge tests between 0.002 and 1.5 V versus Li^+/Li using a multichannel battery testing system (AcuTech Systems BAT-750B).

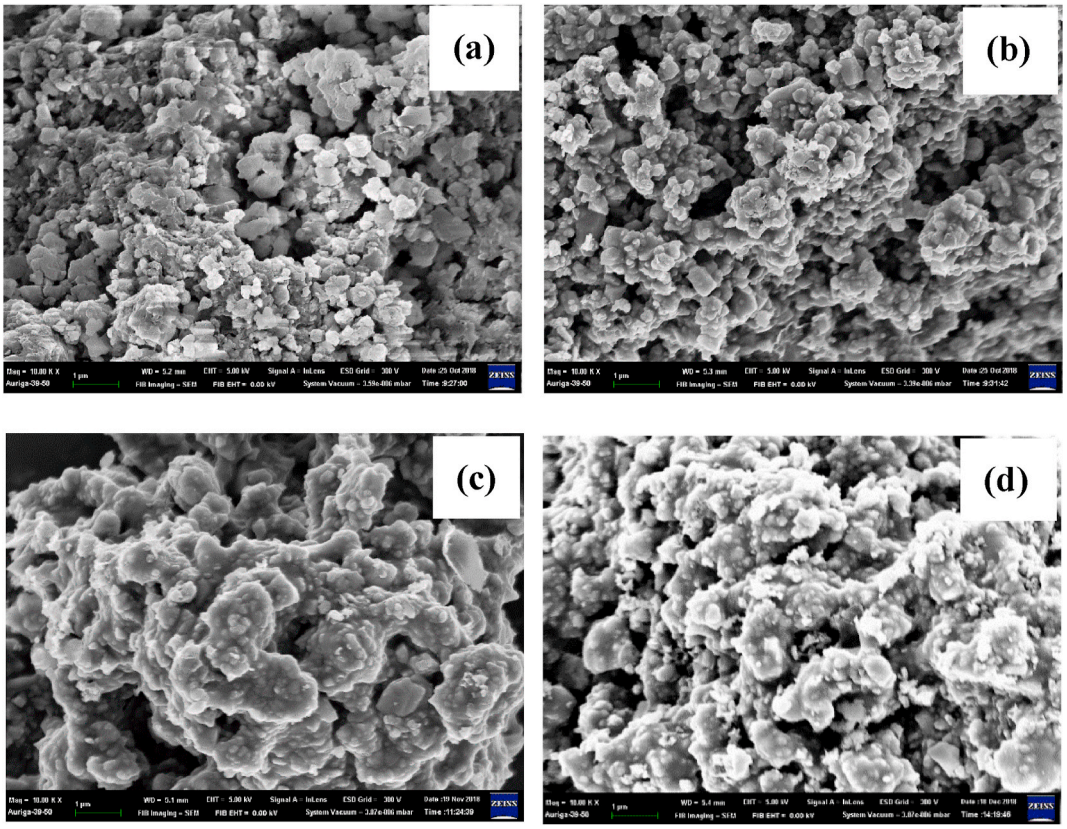

Fig. 2. SEM images of CPC/Si composites. (a) CPC/Si, (b) CPC/Si-700, (c) CPC/Si-800, (d) CPC/Si-900.

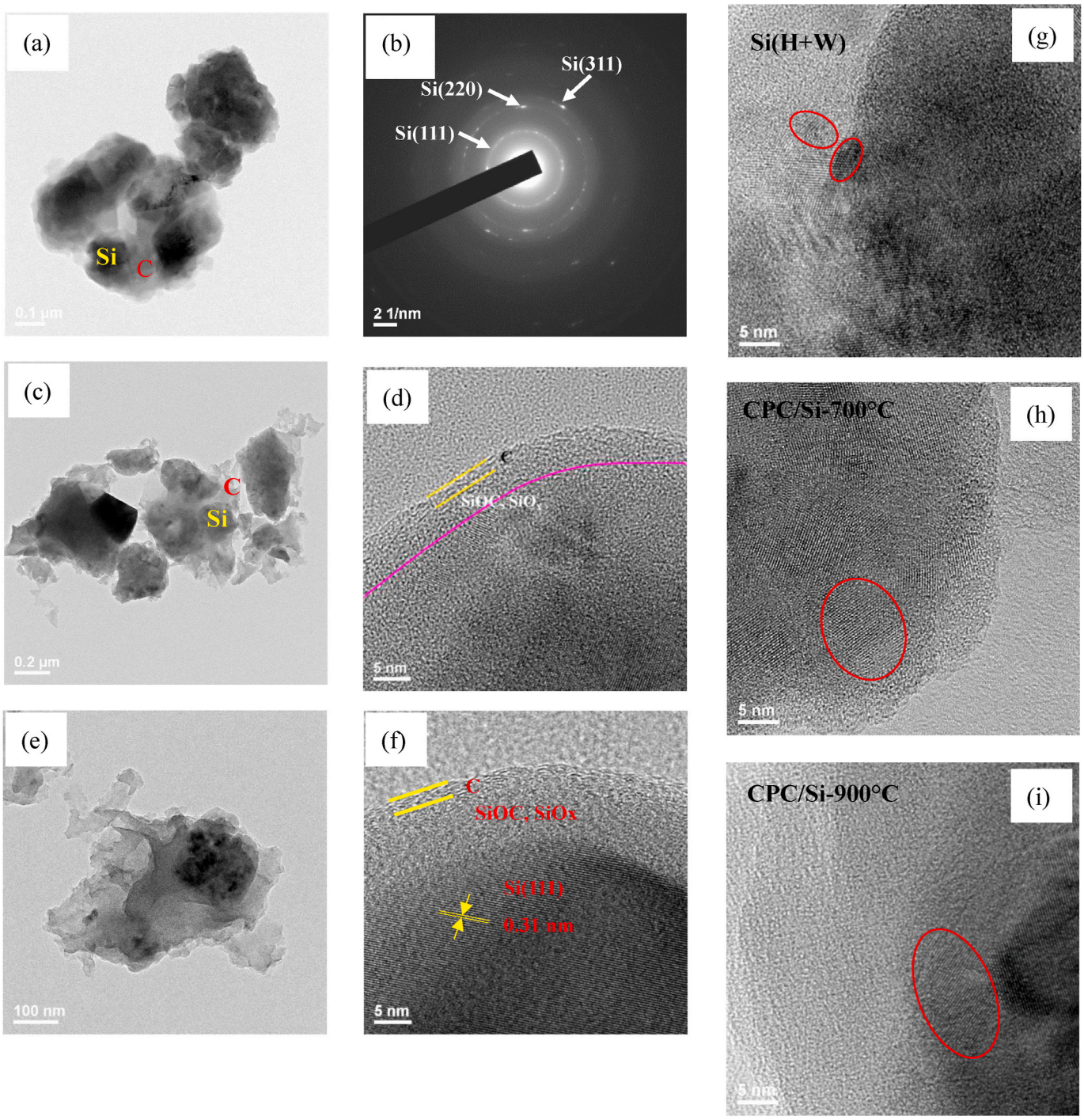

Fig. 3. CPC/Si composite (a) TEM image, (b) SAED pattern. CPC/Si-700 (c) TEM images (d) HRTEM image, CPC/Si – 900 °C (e) TEM image, (f) HRTEM image. HRTEM images of (g) Si, (h) CPC/Si-700, and (i) CPC/Si-900 composites.

3. Results and discussion

The XRD spectra (Fig. 1) revealed a broad XRD peak within 10°–30° for the CPC resin (Fig. 1a) confirming the amorphous character of the as-obtained CPC resin, where the annealing at 900 °C for 2 h led to two obvious peaks at 25° and 45° (Fig. 1b), indicating the short-range ordered carbon material in the CPC resin. The XRD pattern of the pure Si powder (Fig. 1c) matched the standard database well (JCPDS card No. 27–1402), where the XRD peaks at 28.44°, 47.30°, 56.12°, 69.13°, and 76.38° corresponded to the (111), (220), (311), (400), and (331) planes, respectively [23]. The intensity of the XRD peaks decreased, and the peak broadened in the CPC/Si composites (Fig. 1d), which may have been due to the reduction in the size of the Si (16.84 nm obtained from Scherer formula) after ball milling. However, annealing at high temperatures (700 °C, 800 °C, and 900 °C) led to further increases in the intensity of the peaks in the composite (Fig. 1e–g) due to the gradual enhancement of the crystallinity and the size of the Si nanoparticles with increase in annealing temperature. Annealing also led to another broad peak within 15°–25° (as shown by the arrow) corresponding to carbon and silicon oxide (SiOx) [39,40]. The molecular structure of CPC and the formation of the carbon during annealing was confirmed from the thermo-gravimetric analysis (TGA) (Fig. s1, supplementary information)

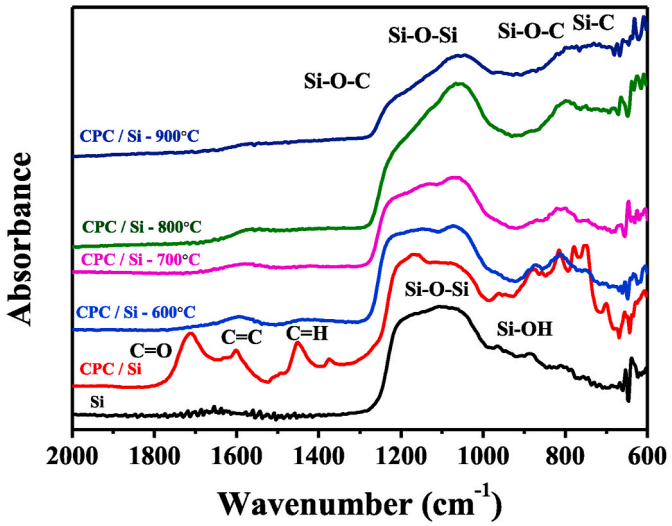

Fig. 4. FTIR spectrum of the Si, CPC/Si composite, and annealed CPC/Si composite.

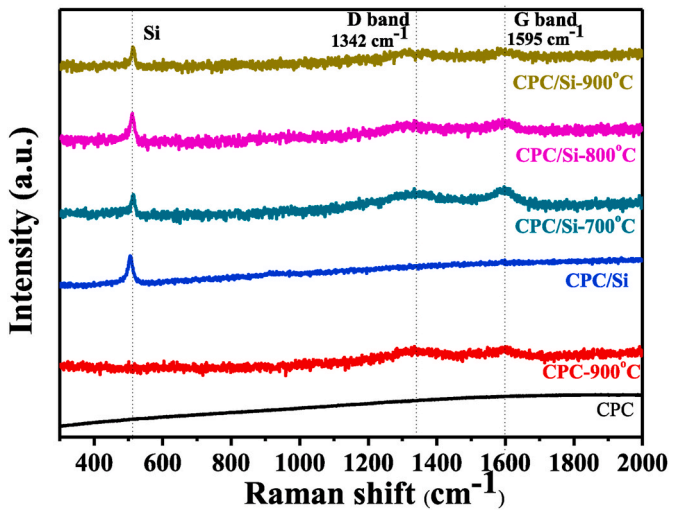

Fig. 5. Raman spectrum of the (a) CPC resin, (b) CPC resin-900 °C, (c) CPC/Si composite, (d) CPC/Si-700 °C, (e) CPC/Si-800 °C, and (f) CPC/Si-900 °C.

of the CPC and the CPC/Si composite. The FE-SEM images (Fig. 2) showed the microstructure of the CPC/Si composites, where the particle size of the composite appeared to increase from ~0.5–0.8 μm in the as-prepared composite and led to large, irregularly shaped ~ 1–2 μm particles after the heat treatment, which increased the crystallization as well as the grain growth. The TEM image (Fig. 3a) of the as-prepared CPC/Si composite confirmed the coating of the silicon particles with the hydrocarbon resin and the corresponding SAED (selected area electron diffraction) in Fig. 3b reveals the polycrystalline nature of the silicon. The diffraction rings correspond to the (111), (220), and (311) planes of Si, and the diffused, low intense ring is from the amorphous carbon in the hydrocarbon resin. The annealed CPC/Si composite (700 °C, and 900 °C) (Fig. 3c,e) exhibits a color contrast which distinguishes the Si and carbon. The darker contrast is the Si particles with smooth edges, and the carbon has a lighter contrast with uneven edges. The composite used carbon as the basic frame with Si embedded in the matrix to form a silicon-carbon composite material. The high-resolution (HR-TEM) images of the composite material annealed at 700 °C and 900 °C (Fig. 3d,f) confirm the formation of three different layers, with carbon as the outermost layer, the amorphous SiOC/SiOx at the interface, followed by Si showing a clear distinct (111) crystal plane (d spacing = 0.31 nm). There is an obvious increase in the particle size of the Si from ~10 nm for $Si_{(H+W)}$, to ~30 nm (700 °C), ~40 nm (900 °C) with the increase of the annealing temperature (Fig. 3g-i). The HR-TEM analysis confirmed the successful synthesis of the silicon-carbon composite material with carbon as a buffer and with Si embedded in the matrix, and the interface between silicon and carbon contained SiOC/-SiOx. It may be mentioned that the SiOC layer might form at the SiO_X-C interface at high annealing temperatures (900 °C). Usually, SiOC layer is amorphous below 1000 °C [41] and it is very difficult to observe this layer by HRTEM. However, FTIR and XPS analysis confirmed the presence of SiOC layer in the annealed CPC/Si composite. Nevertheless, the Si with the surrounding carbon materials can act as a buffer in the composite and slow down the volume expansion and contraction in the silicon while providing good conductivity that optimizes battery performance.

The FTIR spectra (Fig. 4) of all the as-obtained materials and annealed silicon-carbon composite revealed several absorption bands, where the spectrum corresponding to pure Si revealed an Si–O–Si bond (1000–1200 cm^{-1}) and an Si–OH bond (800-900 cm^{-1}). The CPC/Si composite comprised a few other bands at 1700 cm^{-1} (C═O), 1600 cm^{-1} (C═C), and 1450 cm^{-1} (C–H), where the bands at low wavenumbers (850 cm^{-1}, 1200 cm^{-1} (Si–O–C) [42,43] and 730 cm^{-1} (Si–C)) [42,43] were related to various bond vibrations of Si–C in addition to the Si–O–Si bond at 1050 cm^{-1} [42–44]. The FTIR analysis verified that the addition of PAA as a bonding agent between hydrocarbon resin and silicon powder during ball milling is a good method to use for the preparation of a silicon-carbon composite. The un-annealed and annealed silicon-carbon composites confirmed the elimination of the C═O and C–H functional groups after the heat treatment. The as-prepared CPC/Si composite had more Si-OC bonds, and further, with increases in the annealing temperature (700 °C–900 °C), the original oxygen bonded to carbon atoms was more inclined to bond with the silicon, leading to an increase in the Si–O–Si bonding. The silicon-carbon composite material generated an Si–C bond (700-800 cm^{-1}) after high temperature heat treatment, as observed in both CPC/Si composites annealed at 800 °C and 900 °C, respectively. Since the silicon-carbon composites undergo high temperature heat treatment, the silicon-carbon interface may react at high temperatures to form SiOC at 800 °C.

The Raman spectrum (Fig. 5) of the hydrocarbon resin exhibited a smooth curve without any D or G band, indicating that the amorphous nature of the carbon and the crystallinity of the material increased with the emergence of the D-band and G-band after the heat treatment at 900 °C. Typically, the peak at 1342 cm^{-1} is designated as the D-band (sp^3 bonds of the carbon), where its strength represents the concentration of the defects in the material structure [45]. The G band at 1595 cm^{-1} describes the stable sp^2 bonded carbon atoms, where the intensity ratio (I_D/I_G) between the D-band and G-band is typically used as a basis to estimate the degree of disorder in carbon materials. A CPC/Si composite without any heat treatment had a characteristic peak at 520 cm^{-1} corresponding to silicon without any D or G-band. This was observed in all of the CPC/Si composites after heat treatment at 700 °C, 800 °C, and 900 °C. The intensity ratio (I_D/I_G) of the CPC/Si composite decreased (2.83 at 700 °C to 1.26 at 900 °C) with increases in the annealing temperature, indicating a gradual decrease in the defect concentration in the composite. In the electrochemical reaction, if the carbon material has a high amount of defects, this is more conducive to the diffusion/-storage of lithium ions.

The C_{1s} XPS spectra (Fig. 6, Table 1a) for the CPC/Si composites after deconvolution had C–C (284.6 eV), C–O (285.4 eV), O–C═O (288.8 eV) bonds, where the intensity of the C–C (C–O) bond increased (decreased) with increases in the annealing temperature. In addition to the reduction of the hydrocarbon resin with increases in temperature, the C–O content in the CPC/Si-700 °C composites was 39.63%, which decreased gradually to 25.65% and 24.43% for the composites annealed at 800 °C and

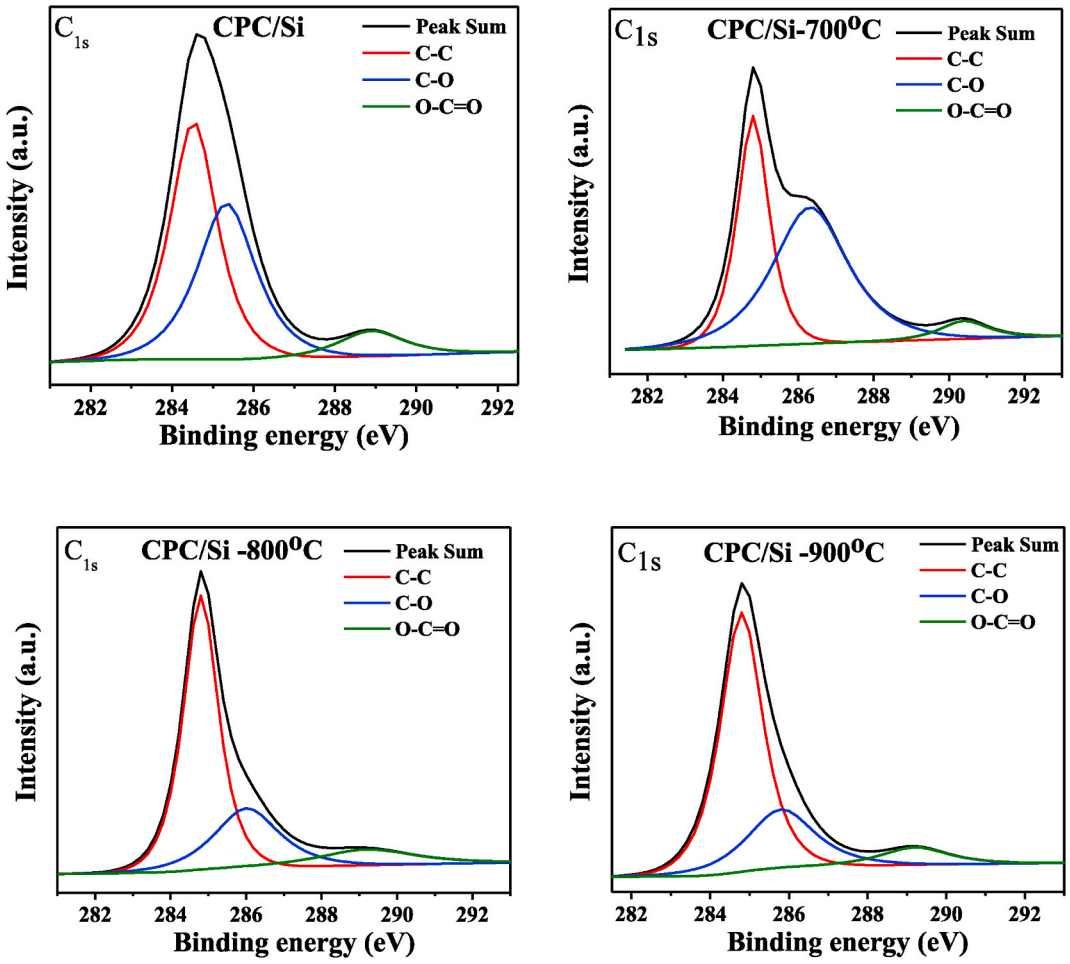

Fig. 6. ESCA spectrum of the C 1s for un-annealed and annealed CPC/Si composites.

Table 1a
C 1s ESCA data.

Sample	Chemical Bond	Concentration (%)
CPC resin	C – C	44.08
	C – O	37.57
	O – C = O	18.35
CPC/Si - 700 °C	C – C	55.69
	C – O	39.63
	O – C = O	4.68
CPC/Si - 800 °C	C – C	64.21
	C – O	25.65
	O – C = O	10.14
CPC/Si - 900 °C	C – C	68.29
	C – O	24.43
	O – C = O	7.28

900 °C, respectively. The oxidation of Si increased significantly for CPC/Si-800 °C and CPC/Si-900 °C, and it appeared that the oxygen atoms bonded with carbon tended to be more bonded with silicon to form SiO_x. The Si 2p XPS spectra (Fig. 7) confirmed the different oxidation states at binding energies of 99.4 eV(Si–C), 100.4 eV($SiOC_3$), 101.4 eV (SiO_2C_2), 102.5 eV (SiO_3C) and 103.6 eV (SiO4) [41,46,47] (Table1b) and that agrees well with the previously published report. The un-annealed CPC/Si composite material was 37.14% un-oxidized silicon (Si^0), which dropped to 9.47% at 700 °C, 4.05% at 800 °C, and 3.2% at 900 °C. Similarly, the Si^{3+} (Si^{4+}) content increased consistently from 20.95% (12.75%) for CPC/Si to 34.42% (14.98%), 51.81% (27.82%), 51.54% (28.52%) with increases in the annealing temperature from 700°C to 900 °C. The Si 2p spectra were de-convoluted to determine the silicon-to-carbon/oxygen coordination [48]. Table 1b shows a significant difference in the amount of oxidation of the silicon, particularly in the Si^{2+}, Si^{3+}, and Si^{4+} content in the silicon-carbon composites with increases in the heat treatment temperatures (700 °C, 800 °C, and 900 °C), indicating the formation of mixed SiC_xO_{4-x} (mostly x = 0–3)/SiOC material [42,48–50] at the silicon-carbon interface due to the high temperature reaction. According to the literature, SiO_3C can correspond to the Si^{3+} valence electron state [50], which is consistent with the high temperature-annealed CPC/Si composite having a higher Si^{3+} content.

Fig. 8a-c illustrates the charge/discharge spectra for the first three cycles in the silicon-carbon composite annealed at different temperatures. The first cycle charge/discharge capacity was 2291/1846 mAh g^{-1}, 1784/1385 mAh g^{-1}, and 1702/1313 mAh g^{-1} for the composite annealed at 700 °C, 800 °C, and 900 °C respectively. The decline in the capacity was due to the oxidation of the Si surface due to hydrocarbon pyrolysis at a high annealing temperature based on the theoretical assumption that the silicon oxide [39] or SiOC [51] was less than pure silicon. SiO_x was reduced to Si by reacting with lithium ions, with the formation of Li_2O and lithium silicate compounds (Li_4SiO_4, $Li_2Si_2O_5$) through a series of irreversible chemical reactions [12,39,52,53] leading to a loss of capacity. Among the annealed CPC/Si composites, CPC/Si-700 °C showed the high first cycle CE of 80.6%, which gradually decreased to 77.7% and 77.2% with increases in the heat treatment temperature due to the oxidation of silicon. However, the literature suggests that the irreversible formation of Li_2O and Li_4SiO_4 can allow them to serve as a buffer during the volume expansion or contraction of

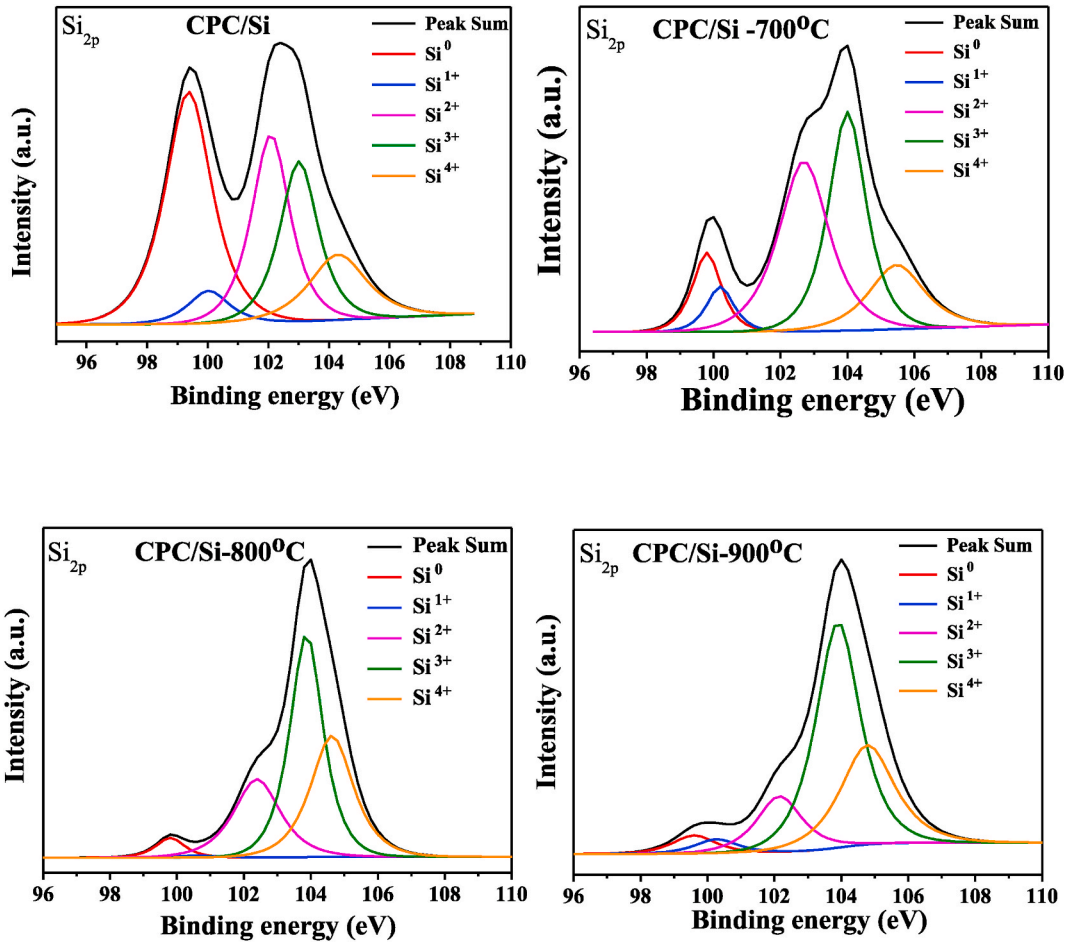

Fig. 7. ESCA spectrum of the Si 2p for un-annealed/annealed CPC/Si composites.

Table 1b
ESCA data for the Si 2p.

Sample	Si^0 (%)	Si^{1+} (%)	Si^{2+} (%)	Si^{3+} (%)	Si^{4+} (%)
CPC/Si	37.14	4.57	24.59	20.95	12.75
CPC/Si −700 °C	9.47	5.18	35.95	34.42	14.98
CPC/Si −800 °C	4.05	3.09	13.23	51.81	27.82
CPC/Si −900 °C	3.20	3.44	13.30	51.54	28.52

Si during the charge discharge cycles. In addition, SiOC material undergoes a non-alloying reaction mechanism [42], thereby improving the cyclic stability of the battery [54–56]. The pure Si, as usual, showed a high charge/discharge capacity of 3975 mAh g^{-1} (3526 mAh g^{-1}) in the first cycle, which decreased gradually to 3609 mAh g^{-1} (3040 mAh g^{-1}) and 3090 mAh g^{-1} (2940 mAh g^{-1}) in the second and third cycles (Tables 1 and 2), respectively. Similarly, the columbic efficiency (CE) for the first, second, and third cycle was ~88.7%, 84.2% and 95.1%, respectively. Table 2 summarizes the charge and discharge capacity and the coulomb efficiency of all the composites. The corresponding cyclic voltammogram for the first five cycles (scan rate = 0.1 mV/s, voltage range = 0–2 V) is presented in Fig. 8d-f. The broad peak ranging from 0.5 V–1.2 V in the first anodic (insertion lithium) cycle of all the composites that disappears in the 2nd cycle gives an idea of the formation of the SEI film on the electrode surface, where the peak below 0.3 V is attributed to the insertion of Li ions into Si [22,57]. The first discharge cycle does not show the reduction peak at 0.2 V, which appears at 0.15 V from the 2nd cycle and becomes more prominent with increases in the number of charge/discharge cycles due to the formation of a series of lithium-silicon alloys during the lithiation of amorphous silicon (Li_xSi). Two broad oxidation peaks at 0.36 V and 0.53 V in the first to fifth cycles are ascribed to the partial decomposition of Li_xSi and the extraction of Li ions from the silicon host, respectively [22,57]. The increase in the intensity of both the oxidation and reduction peaks is due to the activation of the Si phase during the charge/discharge process.

Fig. 9a and Table 3 compare the cyclic stability of the pure silicon and CPC/Si composites annealed at different temperatures. Among all the CPC/Si composites, those annealed at 600 °C and 700 °C show a gradual decline in terms of capacity after 25–35 cycles and after 100 cycles, the discharge capacity reaches 1301 mAh g^{-1} (600 °C) and 1402 mAh g^{-1} (700 °C) with retention of 67.5% and 76%, respectively. The composites annealed at high temperatures (800 °C and 900 °C) also exhibited low capacity (1330 mAh g^{-1}, 1340 mAh g^{-1}) after 100 cycles, but, with better retention (96%, 102%) as compared to other composites. This may have been due to the thick, complete carbon layer modified on the Si surface with higher Si–O that contributed to the lower first discharge capacity. Although, pure silicon had achieved the highest discharge of 2485 mAh g^{-1} after 100 charge/discharge cycles, the retention (70.5%) was low as compared with CPC/Si-700.

Fig. 9b and Table 4 present the rate capability of the CPC/Si composites (700 °C, 800 °C, and 900 °C) where the electrodes were charged/discharged at a rate of 0.1C for eight cycles to ensure the generation of a stable SEI film in the half-cell. The rate was gradually increased to 2C to check the stability of the composite at a high current rate, after which it was reversed back to 0.1C to confirm reproducibility. Among all the composites, the CPC/Si-700 °C had the highest capacity of 1998 mAh g^{-1} at 0.1C during the first eight cycles, decreasing gradually to 1396 mAh g^{-1} (1020 mAh g^{-1}) at 1C (2C) after 23 (28) cycles. The capacity

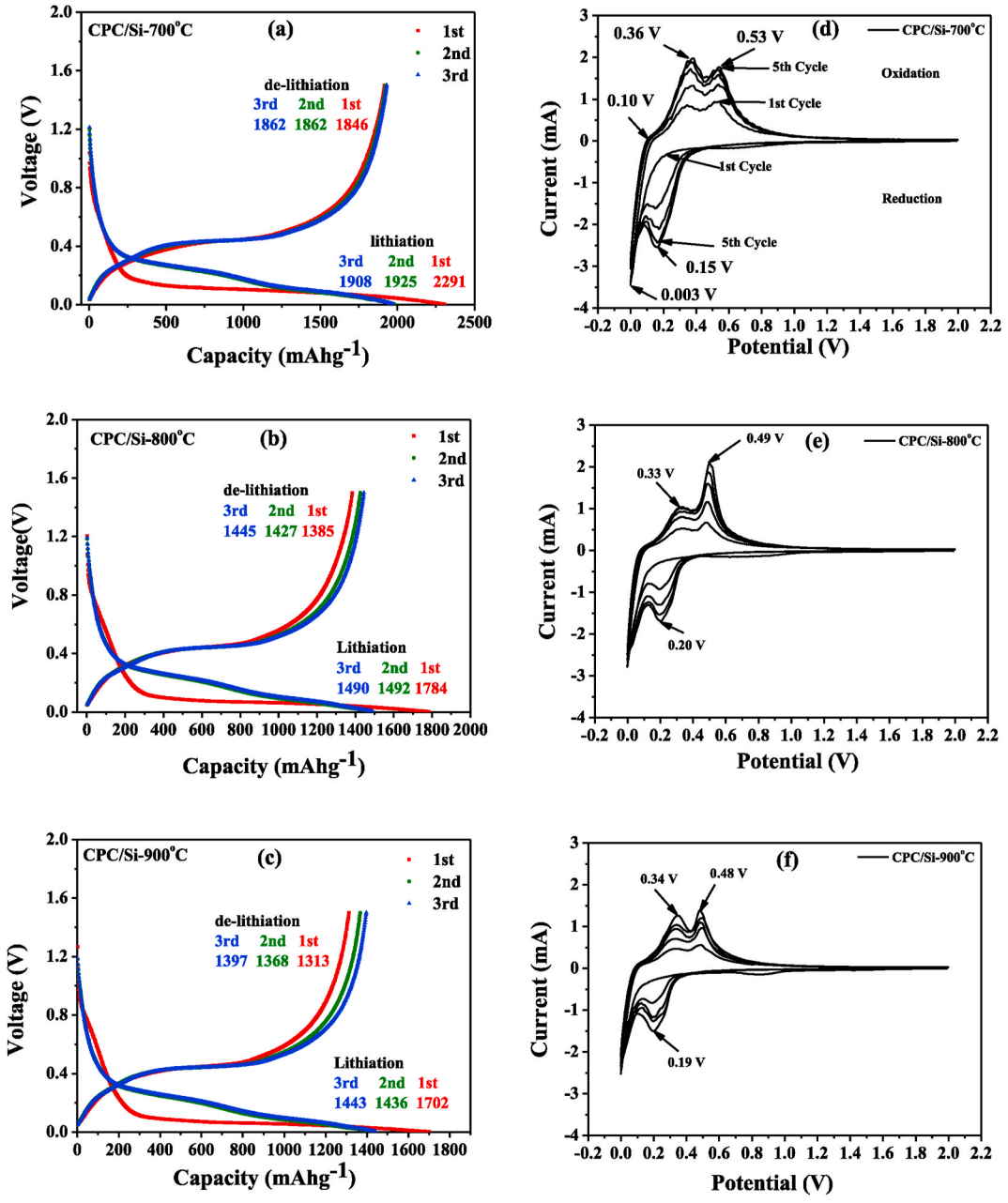

Fig. 8. Charge/discharge (a–c) and the CV analysis (d–f) of CPC/Si composites annealed at 700 °C, 800 °C, and 900 °C.

Table 2
Electrochemical properties of the bare Si and (1:1) CPC/Si composite.

Si				CPC/Si-700 °C			
Cycle	Charge Capacity (mAh/g)	Discharge Capacity (mAh/g)	C.E. (%)	Cycle	Charge Capacity (mAh/g)	Discharge Capacity (mAh/g)	C.E. (%)
1st	3975	3526	88.7	1st	2291	1846	80.6
2nd	3609	3040	84.2	2nd	1925	1862	96.7
3rd	3090	2940	95.1	3rd	1908	1862	97.6
CPC/Si-800°C				**CPC/Si-900°C**			
Cycle	**Charge Capacity (mAh/g)**	**Discharge Capacity (mAh/g)**	**C.E. (%)**	**Cycle**	**Charge Capacity (mAh/g)**	**Discharge Capacity (mAh/g)**	**C.E. (%)**
1st	1784	1385	77.7	1st	1702	1313	77.2
2nd	1492	1427	95.7	2nd	1436	1368	95.3
3rd	1490	1445	97.0	3rd	1443	1397	96.8

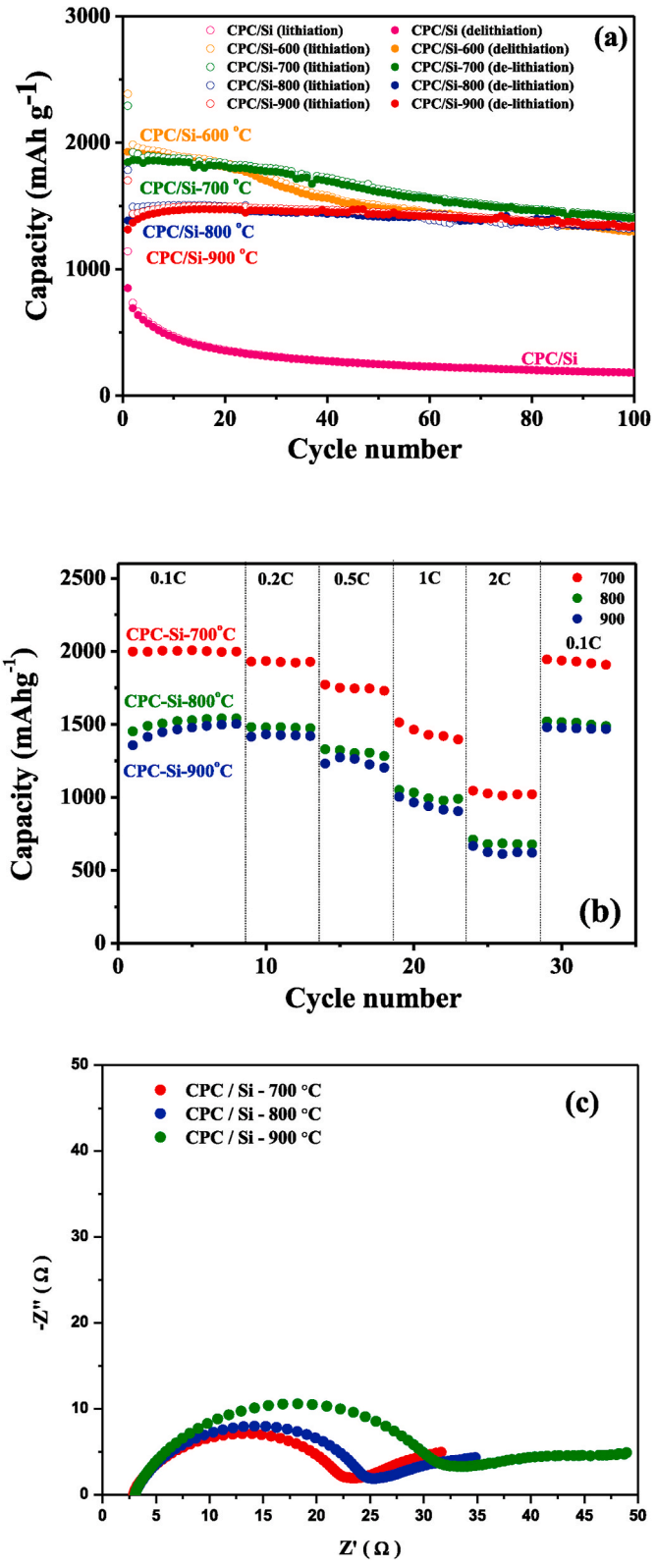

Fig. 9. (a) Cycling performance of bare Si and CPC/Si composites at a current density of 0.1 C, (b) C-rate test of CPC/Si composites annealed at 700 °C, 800 °C and 900 °C, (c) EIS analysis of the CPC/Si composites.

recovered to ~1908 mAh g^{-1} at 0.1C. Enhanced capacity at a high charge/discharge rate (1020 mAh g^{-1} at 2C) and much better retention (95%) after 33 cycles confirmed the physical/chemical stability of the composite. The other CPC/Si composites (Table 4) annealed at 800 °C

Table 3
Cyclic stability data for the Si and CPC/Si composites.

	1st charge (mAh g^{-1})	1st discharge (mAh g^{-1})	100th discharge (mAh g^{-1})	Retention (%)
Si	3975	3526	2485	70.5
CPC/Si	1141	850	181	21.3
CPC/Si-600 °C	2386	1927	1301	67.5
CPC/Si-700 °C	2291	1846	1402	76
CPC/Si-800 °C	1784	1385	1330	96
CPC/Si-900 °C	1702	1313	1340	102

Table 4
C-rate test for the CPC/Si composites.

	0.1 C	0.2 C	0.5 C	1 C	2 C	0.1 C	Retention (%)
CPC/Si-700°C	1998	1927	1729	1396	1020	1908	95.5
CPC/Si-800°C	1540	1473	1282	989	676	1488	96.6
CPC/Si-900°C	1502	1419	1204	904	619	1468	97.7

(676 mAh g^{-1} at 2C) and 900 °C (619 mAh g^{-1} at 2C) exhibited very good capacity as well as cyclic stability with very good retention of ~97%.

Fig. 9c shows the AC impedance spectra of the CPC/Si composite after the fifth cycle and illustrates four different resistances. The first one is the overall series resistance (Rs) generated at the electrode surface due to the transport of the electron in the active material between the particles of the active material and transport of the Li ion in the electrolyte. The high frequency semicircle corresponds to the resistance generated by the SEI layer (R_{SEI}). The second semicircle in the intermediate frequency region is attributed to charge transfer resistance (Rct) due to the reaction at the interface of the electrolyte. The active material and (d) the Warburg impedance in the low frequency region is due to the Li ion diffusion in the electrode [22]. The impedance spectra shows an increase in the resistance of the SEI film and the charge transfer resistance with increases in the annealing temperature of the composite, which hindered the Li ion transport in the active material. The composite annealed at 700 °C had much lower SEI and charge transfer resistance as compared to the other composites. The formation of the low SEI is probably related to the annealing temperature where the CPC/Si annealed at 700 °C led to the formation of the thinner SiOC/SiOx layer than in CPC/Si-900 (Fig. s2-supplementary information). Lower annealing temperature for CPC/Si-700 had suppressed the growth of SiOC/SiOx having lower conductivity than silicon resulting in lower SEI and charge transfer resistance in CPC/Si-700. It achieved better electrochemical performance, as shown by its high capacity and much better rate capability. Table 5 summarizes the battery performance of Si/C composite with the earlier reports that suggests the potential of this composite as an anode in LIBs.

Therefore, modification of silicon through carbon served as a framework in which to buffer the volume expansion and contraction of silicon during the charge/discharge cycles. At the same time, the outer carbon layer formed on the surface of the silicon prevented the formation of unstable SEI films and maintained the structure of the silicon-carbon composite material. In addition, the increase in the ratio of SiOC to SiOx reduced the overall capacity of the composite, but the volume expansion rate of SiOC and SiOx during the lithiation process was nearly 150–200%, which was significantly smaller than that of pure silicon. The Li_2O and Li_4SiO_4 formed by the irreversible electrochemical

Table 5
Summary of earlier reports on Si/carbon nanocomposites.

Authors	Anode materials	Synthesis procedure	Composite morphology/size	Discharge capacity after 100 cycles (mAh/g)	Current rate (mA/g or C)	Voltage range (V)	Capacity retention %	Ref.
Huang et al. Our work	Si/C	Ball milling of Si powder with CPC resin and anneal at high temperature (600 °C–900 °C)	Si particle covered with C layer	1402 mAhg^{-1} after 100 cycles	0.1C	0–2	76	
Pan et al.	Si/C	Polydopamine coating on Si nanoparticle followed by annealing in Ar atmosphere	Yolk–shell structure	804 mA h g^{-1} after 50 cycles	1Ag^{-1}	0–2	83	[23]
Shao et al.	Si/porous C	Multiple steps involving dispersion Si nanopartilces in an aqueous solution of Pluronic F127 and glucose, hydrothermal process and carbonization	Si-porous C sphere	1607 mA hg^{-1} after 100 cycles	0.4 A g^{-1}	0–2	85	[22]
Chen et al.	Silicon core–hollow carbon shell nanocomposites	Several steps including pre-paration of Si@SiO_2 core–shell nanoparticles followed by coating with polydopami ne and annealing at 900 °C	Silicon core–hollow carbon shell nanocomposites	1625 mA hg^{-1} after 100 cycles	0.05 C	0–2	69	[58]
Li et al.	porous Si–C nanocomposites	Calcination of Si nanopowder to form SiO_2 layer on Si followed by coating of thin layer of amorphous carbon Etching of Si@SiO_2@C composite in HF solution to form porous Si–C nanocom-posites	hollow core–shell structure	650 mA hg^{-1} after 100 cycles	0.4 A g^{-1}	0–2	86	[35]
Liu et al.	Si–C nanocomposites	Si nanoparticle was coated with SiO2 as sacrificial layer and polydopamine coating followed by carobonization to form N doped carbon and removal of SiO2 by HF etching	Si@void@C particles	~1500 mA hg^{-1} after 1000 cycles	1C	0–2	74	[21]
Magasinski et al.	Si–C nanocomposites	Synthesis of Si nanoparticles on the surface of C black nanoparticles by CVD	Spherical granule like upon carbon coating with Si nanoparticles embeded	1590 mA hg^{-1} after 100 cycles	1C	0–2	82	[20]

reaction can be used as a buffer for the volume expansion/contraction of silicon, in order to maintain a stable structure leading to excellent performance of CPC/Si composite in lithium ion batteries.

4. Conclusion

We used an easy, simple ball milling method along with a heat treatment procedure to synthesize CPC/Si composites, which achieved promising electrochemical performance. These composites are a suitable alternative to graphite for applications in lithium ion batteries. Specifically, the composite annealed at 700 °C had superior first cycle discharge capacity (2291 mAh g^{-1}), appreciable cyclic stability (1402 mAh g^{-1} after 100 cycles with 76% retention), and significantly high rate capabilities (1020 mAh g^{-1} at 2C with retention 95.5%) at a very high current rate. The composites annealed at 800 °C (900 °C) showed remarkable capacity 1330 mAh g^{-1} (1340 mAh g^{-1}) after 100 cycles with 100% retention. The in situ-generated Li_2O and lithium silicates during the first lithiation buffered the large volume change and led to improved cycling stability. Variations in the annealing temperature demonstrated a mixed response for the capacity, cyclic stability, and rate capability of the composites, which may have been due to the carbonization of the carbon layer and subsequently, the change in the oxidation state between Si and carbon forming SiOx and SiOC on the surface of Si. For example, increasing the annealing temperature led to a consistent decrease in the discharge capacity and rate capability, but increased the retention after 100 cycles, which may have been due to the variations in the oxidation of Si, SiOC, and carbonization in the carbon layer.

CRediT authorship contribution statement

Wen-Ya Chung: Investigation, Data curation, Formal analysis. **Sanjaya Brahma:** Formal analysis, Visualization, Data curation, Writing - original draft, Writing - review & editing. **Shang-Chieh Hou:** Formal analysis, Writing - review & editing. **Chia-Chin Chang:** Supervision, Conceptualization, Methodology, Writing - review & editing, Project administration, Funding acquisition. **Jow-Lay Huang:** Supervision, Conceptualization, Resources, Methodology, Project administration, Funding acquisition, Writing - review & editing.

Declaration of competing interest

The authors declare that they have no known competing financial interests or personal relationships that could have appeared to influence the work reported in this paper.

Acknowledgement

This work was financially supported by the Hierarchical Green-Energy Materials (Hi-GEM) Research Center, from The Featured Areas Research Center Program within the framework of the Higher Education Sprout Project by the Ministry of Education (MOE) and the Ministry of Science and Technology (Grant No. MOST 107-3017-F-006 -003, MOST 107-2622-E-024-003-CC2, MOST 108-2622-8-006-014, MOST 109-3116-F-006 -018, MOST 109-2923-E-007-005, MOST 109-2622-8-006-005, MOST 109-2622-8-024-001-TE4, MOST 109-3116-F-006-018, MOST 109-2622-E-024-003-CC2 and MOST 109-2634-F-006 -020) in Taiwan.

Appendix A. Supplementary data

Supplementary data to this article can be found online at https://doi.org/10.1016/j.matchemphys.2020.124011.

References

[1] J. Liang, Z. Zhang, W. Yang, X. Li, P. Li, X. Guo, Y. Jung, X. Dong, Nitrification protection of Si monocrystal nanoparticles into the graphene matrix as the high-performance anode material for lithium-ion batteries, Mater. Chem. Phys. (2020) 123156.

[2] S.-H. Moon, S.-J. Kim, M.-C. Kim, J.-Y. So, J.-E. Lee, Y.-K. Shin, W.-G. Bae, K.-W. Park, Stress-relieved Si anode on a porous Cu current collector for high-performance lithium-ion batteries, Mater. Chem. Phys. 223 (2019) 152–156.

[3] H.-C. Tao, X.-L. Yang, L.-L. Zhang, S.-B. Ni, Chemically activated graphene/porous Si@ SiOx composite as anode for lithium ion batteries, Mater. Chem. Phys. 147 (2014) 528–534.

[4] L. Wang, T. Mei, W. Liu, J. Sun, Q. Zhou, Y. Qian, Low temperature chemical synthesis of silicon nanoparticles as anode materials for lithium-ion batteries, Mater. Chem. Phys. 220 (2018) 308–312.

[5] B. Jang, J. Koo, S. Choi, J. Kim, Formation of SiOx shell on Si nanoparticles and its effects on electrochemical properties as a Li-ion battery's anode, Mater. Chem. Phys. 215 (2018) 11–19.

[6] Y.-Z. Wu, S. Brahma, S.-C. Weng, C.-C. Chang, J.-L. Huang, Reduced graphene oxide (RGO)-SnOx (x= 0, 1, 2) nanocomposite as high performance anode material for lithium-ion batteries, J. Alloys Compd. 818 (2020) 152889.

[7] C.-C. Hou, S. Brahma, S.-C. Weng, C.-C. Chang, J.-L. Huang, Facile, low temperature synthesis of SnO2/reduced graphene oxide nanocomposite as anode material for lithium-ion batteries, Appl. Surf. Sci. 413 (2017) 160–168.

[8] C.-C. Hou, S. Brahma, S.-C. Weng, C.-C. Chang, J.-L. Huang, Multi-layer graphene/SnO2 nanocomposites as negative electrode materials for lithium-ion batteries, Journal of Electrochemical Energy Conversion and Storage 17 (2020).

[9] S.-C. Weng, S. Brahma, C.-C. Chang, J.-L. Huang, Synthesis of self-assembled hollow-sphere ZnO/rGO nanocomposite as anode materials for lithium-ion batteries, Int. J. Electrochem. Sci 14 (2019) 3727–3739.

[10] S.-C. Weng, S. Brahma, C.-C. Chang, J.-L. Huang, Synthesis of MnOx/reduced graphene oxide nanocomposite as an anode electrode for lithium-ion batteries, Ceram. Int. 43 (2017) 4873–4879.

[11] S.-C. Weng, S. Brahma, P.-C. Huang, Y.-C. Huang, Y.-H. Lee, C.-C. Chang, J.-L. Huang, Enhanced capacity and significant rate capability of Mn3O4/reduced graphene oxide nanocomposite as high performance anode material in lithium-ion batteries, Appl. Surf. Sci. 505 (2020) 144629.

[12] H. Kim, M. Seo, M.H. Park, J. Cho, A critical size of silicon nano-anodes for lithium rechargeable batteries, Angew. Chem. Int. Ed. 49 (2010) 2146–2149.

[13] C.K. Chan, H. Peng, G. Liu, K. McIlwrath, X.F. Zhang, R.A. Huggins, Y. Cui, High-performance lithium battery anodes using silicon nanowires, Nat. Nanotechnol. 3 (2008) 31.

[14] M.-H. Park, M.G. Kim, J. Joo, K. Kim, J. Kim, S. Ahn, Y. Cui, J. Cho, Silicon nanotube battery anodes, Nano Lett. 9 (2009) 3844–3847.

[15] Y. Yao, M.T. McDowell, I. Ryu, H. Wu, N. Liu, L. Hu, W.D. Nix, Y. Cui, Interconnected silicon hollow nanospheres for lithium-ion battery anodes with long cycle life, Nano Lett. 11 (2011) 2949–2954.

[16] J. Cho, Porous Si anode materials for lithium rechargeable batteries, J. Mater. Chem. 20 (2010) 4009–4014.

[17] S. Fang, L. Shen, G. Xu, P. Nie, J. Wang, H. Dou, X. Zhang, Rational design of void-involved Si@ TiO2 nanospheres as high-performance anode material for lithium-ion batteries, Acs Appl Mater Inter 6 (2014) 6497–6503.

[18] I.-S. Kim, P.N. Kumta, High capacity Si/C nanocomposite anodes for Li-ion batteries, J. Power Sources 136 (2004) 145–149.

[19] J. Shu, H. Li, R. Yang, Y. Shi, X. Huang, Cage-like carbon nanotubes/Si composite as anode material for lithium ion batteries, Electrochem. Commun. 8 (2006) 51–54.

[20] A. Magasinski, P. Dixon, B. Hertzberg, A. Kvit, J. Ayala, G. Yushin, High-performance lithium-ion anodes using a hierarchical bottom-up approach, Nat. Mater. 9 (2010) 353–358.

[21] N. Liu, H. Wu, M.T. McDowell, Y. Yao, C. Wang, Y. Cui, A yolk-shell design for stabilized and scalable Li-ion battery alloy anodes, Nano Lett. 12 (2012) 3315–3321.

[22] D. Shao, D. Tang, Y. Mai, L. Zhang, Nanostructured silicon/porous carbon spherical composite as a high capacity anode for Li-ion batteries, J. Mater. Chem. 1 (2013) 15068–15075.

[23] L. Pan, H. Wang, D. Gao, S. Chen, L. Tan, L. Li, Facile synthesis of yolk–shell structured Si–C nanocomposites as anodes for lithium-ion batteries, Chem. Commun. 50 (2014) 5878–5880.

[24] Y. Wang, L. Ren, Y. Liu, X. Liu, K. Huang, X. Wei, J. Li, X. Qi, J. Zhong, Carbon matrix/SiNWs heterogeneous block as improved reversible anodes material for lithium ion batteries, Journal of energy chemistry 23 (2014) 105–110.

[25] L. Hu, B. Luo, C. Wu, P. Hu, L. Wang, H. Zhang, Yolk-shell Si/C composites with multiple Si nanoparticles encapsulated into double carbon shells as lithium-ion battery anodes, Journal of Energy Chemistry 32 (2019) 124–130.

[26] Y. Du, M. Hou, D. Zhou, Y. Wang, C. Wang, Y. Xia, Interconnected sandwich structure carbon/Si-SiO2/carbon nanospheres composite as high performance anode material for lithium-ion batteries, Journal of energy chemistry 23 (2014) 315–323.

[27] J. Luo, X. Zhao, J. Wu, H.D. Jang, H.H. Kung, J. Huang, Crumpled graphene-encapsulated Si nanoparticles for lithium ion battery anodes, J. Phys. Chem. Lett. 3 (2012) 1824–1829.

[28] M. Ko, S. Chae, S. Jeong, P. Oh, J. Cho, Elastic a-silicon nanoparticle backboned graphene hybrid as a self-compacting anode for high-rate lithium ion batteries, ACS Nano 8 (2014) 8591–8599.

[29] J. Zhou, N. Lin, Y. Han, J. Zhou, Y. Zhu, J. Du, Y. Qian, Cu 3 Si@ Si core–shell nanoparticles synthesized using a solid-state reaction and their performance as anode materials for lithium ion batteries, Nanoscale 7 (2015) 15075–15079.

[30] J.-S. Lee, M.-S. Shin, S.-M. Lee, Electrochemical properties of polydopamine coated Ti-Si alloy anodes for Li-ion batteries, Electrochim. Acta 222 (2016) 1200–1209.

[31] S. Chae, M. Ko, S. Park, N. Kim, J. Ma, J. Cho, Micron-sized Fe–Cu–Si ternary composite anodes for high energy Li-ion batteries, Energy Environ. Sci. 9 (2016) 1251–1257.

[32] J. Su, C. Zhang, X. Chen, S. Liu, T. Huang, A. Yu, Carbon-shell-constrained silicon cluster derived from Al-Si alloy as long-cycling life lithium ion batteries anode, J. Power Sources 381 (2018) 66–71.

[33] M. Li, J. Qiu, S. Zhang, P. Zhao, Z. Jin, A. Wang, Y. Wang, Y. Yang, H. Ming, Micrometre-sized ferrosilicon composites wrapped with multi-layered carbon nanosheets as industrialized anodes for high energy lithium-ion batteries, Journal of Energy Chemistry (2020).

[34] X. Cao, Y. Fan, J. Qu, T. Wang, D. Legut, Q. Zhang, 2D-layered Sn/Ge anodes for lithium-ion batteries with high capacity and ultra-fast Li ion diffusivity, Journal of Energy Chemistry 47 (2020) 160–165.

[35] X. Li, P. Meduri, X. Chen, W. Qi, M.H. Engelhard, W. Xu, F. Ding, J. Xiao, W. Wang, C. Wang, Hollow core–shell structured porous Si–C nanocomposites for Li-ion battery anodes, J. Mater. Chem. 22 (2012) 11014–11017.

[36] Z. Liu, X. Chang, T. Wang, W. Li, H. Ju, X. Zheng, X. Wu, C. Wang, J. Zheng, X. Li, Silica-derived hydrophobic colloidal nano-Si for lithium-ion batteries, ACS Nano 11 (2017) 6065–6073.

[37] S.-C. Hou, T.-Y. Chen, Y.-H. Wu, H.-Y. Chen, X.-D. Lin, W.-K. Liew, C.-C. Chang, J.-L. Huang, Influence of glucose derivatives on ball-milled Si for negative electrodes with high area capacity in lithium-ion batteries, Acs Sustain Chem Eng 7 (2019) 2971–2979.

[38] S.-C. Hou, Y.-F. Su, C.-C. Chang, C.-W. Hu, T.-Y. Chen, S.-M. Yang, J.-L. Huang, The synergistic effects of combining the high energy mechanical milling and wet milling on Si negative electrode materials for lithium ion battery, J. Power Sources 349 (2017) 111–120.

[39] Q. Si, K. Hanai, T. Ichikawa, M. Phillipps, A. Hirano, N. Imanishi, O. Yamamoto, Y. Takeda, Improvement of cyclic behavior of a ball-milled SiO and carbon nanofiber composite anode for lithium-ion batteries, J. Power Sources 196 (2011) 9774–9779.

[40] J. Sun, Z. Xu, W. Li, X. Shen, Effect of nano-SiO2 on the early hydration of alite-sulphoaluminate cement, Nanomaterials 7 (2017) 102.

[41] M. Halim, G. Liu, R.E.A. Ardhi, C. Hudaya, O. Wijaya, S.-H. Lee, A.-Y. Kim, J.K. Lee, Pseudocapacitive characteristics of low-carbon silicon oxycarbide for lithium-ion capacitors, Acs Appl Mater Inter 9 (2017) 20566–20576.

[42] M. Halim, C. Hudaya, A.-Y. Kim, J.K. Lee, Phenyl-rich silicone oil as a precursor for SiOC anode materials for long-cycle and high-rate lithium ion batteries, J. Mater. Chem. 4 (2016) 2651–2656.

[43] M. Wilamowska-Zawlocka, P. Puczkarski, Z. Grabowska, J. Kaspar, M. Graczyk-Zajac, R. Riedel, G.D. Sorarù, Silicon oxycarbide ceramics as anodes for lithium ion batteries: influence of carbon content on lithium storage capacity, RSC Adv. 6 (2016) 104597–104607.

[44] S.-C. Hou, T.-Y. Chen, Y.-H. Wu, H.-Y. Chen, X.-D. Lin, Y.-Q. Chen, J.-L. Huang, C.-C. Chang, Mechanochemical synthesis of Si/Cu 3 Si-based composite as negative electrode materials for lithium ion battery, Sci Rep-Uk 8 (2018) 1–11.

[45] A.C. Ferrari, J. Robertson, Interpretation of Raman spectra of disordered and amorphous carbon, Phys. Rev. B 61 (2000) 14095.

[46] O. Sublemontier, C. Nicolas, D. Aureau, M. Patanen, H. Kintz, X. Liu, M.-A. Gaveau, J.-L. Le Garrec, E. Robert, F.-A. Barreda, X-ray photoelectron spectroscopy of isolated nanoparticles, J. Phys. Chem. Lett. 5 (2014) 3399–3403.

[47] M. Kim, H. Ju, J. Kim, Oxygen-doped porous silicon carbide spheres as electrode materials for supercapacitors, Phys. Chem. Chem. Phys. 18 (2016) 3331–3338.

[48] H. Fukui, H. Ohsuka, T. Hino, K. Kanamura, A Si− O− C composite anode: high capability and proposed mechanism of lithium storage associated with microstructural characteristics, Acs Appl Mater Inter 2 (2010) 998–1008.

[49] L. David, R. Bhandavat, U. Barrera, G. Singh, Silicon oxycarbide glass-graphene composite paper electrode for long-cycle lithium-ion batteries, Nat. Commun. 7 (2016) 1–10.

[50] Z. Sang, Z. Zhao, D. Su, P. Miao, F. Zhang, H. Ji, X. Yan, SiOC nanolayer wrapped 3D interconnected graphene sponge as a high-performance anode for lithium ion batteries, J. Mater. Chem. 6 (2018) 9064–9073.

[51] A. Wilson, J. Reimers, E. Fuller, J. Dahn, Lithium insertion in pyrolyzed siloxane polymers, Solid State Ionics 74 (1994) 249–254.

[52] B. Guo, J. Shu, Z. Wang, H. Yang, L. Shi, Y. Liu, L. Chen, Electrochemical reduction of nano-SiO2 in hard carbon as anode material for lithium ion batteries, Electrochem. Commun. 10 (2008) 1876–1878.

[53] Q. Sun, B. Zhang, Z.-W. Fu, Lithium electrochemistry of SiO2 thin film electrode for lithium-ion batteries, Appl. Surf. Sci. 254 (2008) 3774–3779.

[54] Y.S. Hu, R. Demir-Cakan, M.M. Titirici, J.O. Müller, R. Schlögl, M. Antonietti, J. Maier, Superior storage performance of a Si@ SiOx/C nanocomposite as anode material for lithium-ion batteries, Angew. Chem. Int. Ed. 47 (2008) 1645–1649.

[55] L. Su, Z. Zhou, M. Ren, Core double-shell Si@ SiO 2@ C nanocomposites as anode materials for Li-ion batteries, Chem. Commun. 46 (2010) 2590–2592.

[56] S. Sim, P. Oh, S. Park, J. Cho, Critical thickness of SiO2 coating layer on core@ shell bulk@ nanowire Si anode materials for Li-ion batteries, Adv. Mater. 25 (2013) 4498–4503.

[57] Y. Xu, G. Yin, Y. Ma, P. Zuo, X. Cheng, Nanosized core/shell silicon@ carbon anode material for lithium ion batteries with polyvinylidene fluoride as carbon source, J. Mater. Chem. 20 (2010) 3216–3220.

[58] S. Chen, M.L. Gordin, R. Yi, G. Howlett, H. Sohn, D. Wang, Silicon core–hollow carbon shell nanocomposites with tunable buffer voids for high capacity anodes of lithium-ion batteries, Phys. Chem. Chem. Phys. 14 (2012) 12741–12745.